Title:

I-M-150847, a novel GLP-1 and GIP receptor dual agonist, reduces body weight gain and improves glycemic control in the rodent model of type 2 diabetes and obesity.

Authors:

Rathin Bauri [$, 1, 2], Shilpak Bele[$, 1, 2], Jhansi Edelli[1], Sourav Dasadhikari[3], Neelesh C.Reddy[4], Sreenivasulu Kurukuti[5], Kanchan Garai[3], Tom Devasia[2], Ahamed Ibrahim[6], Vishal Rai[4], Prasenjit Mitra[1,7†]

[1.] Dr. Reddy's Institute of Life Sciences, University of Hyderabad Campus, Hyderabad, Telangana, India, 500046

[2.] Manipal Academy of Higher Education, Manipal, Karnataka, India -576104.

[3] Tata Institute of Fundamental Research Hyderabad, India, 500046.

[4] Indian Institute of Science Education and Research, Bhopal, 462066

[5]. Department of Animal Biology, University of Hyderabad, India 500046

[6] Division of Lipid Chemistry, National Institute of Nutrition Hyderabad, India 500007.

[7†] corresponding author

[$] Contributed equally.

Correspondence:

prasenjit.mitra01604@gmail.com

Running Title: A novel incretin receptor dual agonist ameliorates diabesity.

Abstract:

We report the discovery of a novel glucagon-like peptide-1 (GLP-1) and glucose-dependent insulinotropic polypeptide (GIP) receptor dual agonist that shows balanced agonism towards both the incretin receptor. The dual agonism of GLP-1 and GIP receptor was achieved by replacing the tryptophan cage of exendin-4 with the C-terminal undecapeptide sequence of oxyntomodulin along with a single amino acid substitution from histidine to tyrosine at the amino terminus of the peptide. The structural modification places lysine 30 of the novel incretin agonist in frame with the corresponding lysine residue in the native GIP sequence. The novel incretin agonist, named I-M-150847, promotes robust glucose-stimulated insulin exocytosis in cultured pancreatic beta cells. Chronic administration of I-M-150847 to mice fed on the high-fat diet improves glucose tolerance, decreases food intake, decreases visceral adiposity and body weight gain demonstrating its therapeutic potential in ameliorating type 2 Diabetes and Obesity.

Significance statement.

- Replacement of the Trp-cage with the C- terminal oxyntomodulin undecapeptide along with the tyrosine substitution at the amino terminus converts the selective GLP-1R agonist exendin-4 to a novel GLP-1R and GIPR dual agonist.
- The GLP-1R and GIPR dual agonist enhances insulin secretion, improve glucose tolerance, reduces food intake, and decreases visceral adiposity and body-weight gain in the rodent model of diabetes and obesity.

Graphical Abstract:

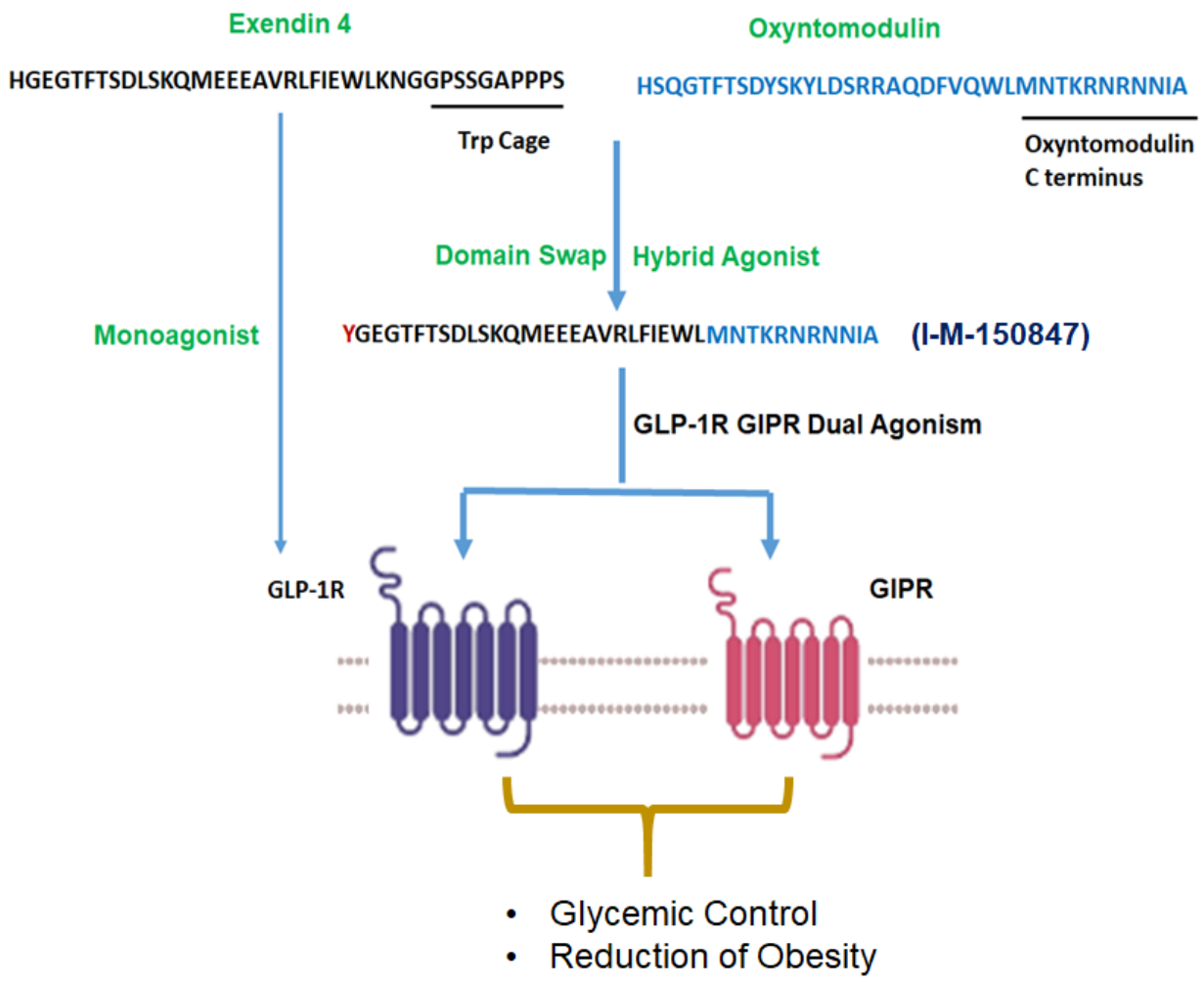

Introduction:

Incretin hormones, glucagon-like peptide-1 (GLP-1), and glucose-dependent insulinotropic polypeptide (GIP) lower the postprandial glucose as they potentiate glucose-stimulated insulin release from the pancreatic beta cells (1),(2). The therapeutic efficacy of GLP-1 is well established (3-5)**,** and epigenetic modulation to amplify GLP-1 receptor (GLP-1R) action has been advocated as an option for the long-term glycemic control and reduction of obesity (6). However, GIP, despite its insulinotropic activity on pancreatic beta cells, has limited clinical relevance as its ability to contain hyperglycemia is diminished in diabetic patients (7), (8).To avail the metabolic benefits of both the incretin receptor agonists, hybrid peptides were designed incorporating residues from GLP-1 and GIP to confer dual GLP-1R and GIPR agonist activity in a single molecule (9-11)**.** The dual agonists exhibit greater efficacy as compared to GLP-1R monoagonists in preclinical settings (10, 12) as well as in the clinical trials (13).

The approach to regulating energy balance through dual agonism exists in nature's repository (14, 15)**.** Oxyntomodulin, an endogenous dual agonist of GLP-1R and Glucagon receptor (GCGR) displays superior bodyweight and glucose-lowering effects than GLP-1 monoagonists upon enhancement of its plasma stability through chemical modifications (16),(17). In a parallel approach, GIP residues were incorporated into the oxyntomodulin sequence to achieve a GIPR, GLP-1R, and GCGR triagonist response in a single hybrid molecule for the development of a potent multi-receptor agonist (18).

In our present report, we employed a structural approach for the rational design of GLP1R and GIPR dual agonists. The crystal structure reveals that the peptide ligands

form alpha-helix as they bind to the extracellular domain of the incretin receptors. The affinity and specificity of the respective ligand and the receptor are determined by the interactions between the amino acid residues of the ligand with that of the binding site of the receptor (19-21). Our data reveal that the replacement of the tryptophan cage (trp-cage) of Exendin-4 tyrosine substituted at the amino terminus (ex-4Y1) with the C terminal undecapeptide sequence of Oxyntomodulin places the lysine 30 of the novel hybrid agonist in frame with the corresponding lysine residue in the native GIP sequence thereby converting the incretin to a GLP-1R-GIPR dual agonist. The novel incretin peptide exhibits potent GLP-1R and GIPR dual agonism with significantly diminished activity towards glucagon receptors. Unlike sustained receptor agonism by GLP-1R agonists (6, 22, 23), the novel dual agonist I-M-150847 induces unique spatiotemporal incretin receptor signaling that promotes cAMP generation at the plasma membrane promoting glucose-stimulated insulin exocytosis. In vivo, I-M-150847 improves glycemic control and reduces the food intake and body weight gain in diet-induced obese mice highlighting its efficacy in regulating metabolic homeostasis.

Results:

Generation of potent GLP-1R and GIPR dual agonists:

Our primary objective was to design a GLP-1R and GIPR dual agonist while minimizing its effect on GCGR. The crystal structure of ligand coupled to GLP-1R and GIPR extracellular domain (19-21), structure-activity relationships of incretins (10, 24, 25), the similarities in their primary sequences as well as the sequence differences in the middle

and the C terminal region of the respective agonists, guided us to rationally design the hybrid peptide with potent GLP-1R and GIPR dual activity in a single molecule. The unimolecular GLP-1R and GIPR dual agonism was achieved in three steps. In the first step, at the C-terminus of the 9- amino acid residue of I-M-150844 that corresponds to the N terminal sequence of exendin-4, we added GIP specific amino acids Tyr^{10}, Ser^{11}, Ile^{12}, Ala^{13}, Met^{14}, Asp^{15}, Lys^{16}, Ile^{17}, His^{18}, Gln^{19}, Gln^{20}, Asp^{21}, Phe^{22}, Val ^{23}, Asn ^{24}, Trp^{25}, and Leu^{26} followed by GLP-1 specific residues Val^{27}, lys^{28}, Gly^{29}, Arg^{30} and Gly^{31} at the C terminal end **(Table 1, Figure 1 Supplementary Fig 3).** The resultant peptide I-M-150845 exhibits 76.78± 6.32% GLP-1R activity, 86.86% ± 13.36 GIPR activity, and 11.5 ± 0.99 % GCGR activity measured in comparison to liraglutide, IUB68, and oxyntomodulin in the corresponding GLP-1R. GIPR and GCGR luciferase reporter assay that indirectly measures cAMP generation. In the next step, we replaced the GLP-1 specific residues Val^{27}, lys^{28}, Gly^{29}, Arg^{30,} and Gly^{31} of I-M-150845 with the C-terminal oxyntomodulin residues Met^{27}, Asn^{28}, Thr^{29}, Lys^{30}, Arg^{31}, Asn^{32}, Arg^{33}, Asn^{34}, Asn^{35}, Ile^{36}, and Ala^{37} to generate a new incretin agonist I-M-150846. The peptide showed 65.65 ± 6.7 % GIPR activity but a drastically attenuated GLP-1R activity **(Table 1, Figure 1 Supplementary Fig 4).**To retain the GLP-1R activity we removed the GIP specific residues Tyr^{10}, Ser^{11}, Ile^{12}, Ala^{13}, Met^{14}, Asp^{15}, Lys^{16}, Ile^{17}, His^{18}, Gln^{19}, Gln^{20}, Asp^{21}, Phe^{22}, Val ^{23}, Asn ^{24} from I-M-150846 and replaced them with exendin-4 specific residues Leu^{10}, Ser ^{11}, Lys^{12}, Gln^{13}, Met^{14}, Glu^{15}, Glu^{16}, Glu^{17}, Ala^{18}, Val^{19}, Arg^{20}, Leu^{21}, Phe^{22}, Ile^{23,} and Glu^{24}. The novel incretin peptide I-M-150847 derived by this replacement exhibited 122.95±2.04% GLP-1R activity, 108.09 ± 5.17 % GIPR activity, and 14.93±1.68% GCGR activity as described in human GLP-1R, GIPR, and GCGR

cell-based cAMP reporter assay (**Table1, Figure 1 Supplementary Fig 5, Fig 1A, B, C**). We next assessed the dose-dependency of I-M-150847 in heterologous human GLP-1R and GIPR assay systems. At 10μM concentration, I-M-150847 has efficacy similar to that of exendin-4, liraglutide, and oxyntomodulin in GLP-1R cell-based cAMP-responsive element luciferase reporter assay. However, at 1μM concentration of I-M-150847, we observed a subtle but significant decrease in activity as compared to exendin-4. **(Fig 1D).** In GIPR cell-based assay, both I-M-150847 and GIPR agonist IUB68 showed comparable efficacy both at 10μM and 1μM concentration of the agonist **(Fig1E).** In contrast, we observed a blunted activity towards GCGR (EC_{50} 53.39μM) in the HEK GCGR cell-based assay system **(Fig 1F).** I-M-150847 exhibits EC_{50} of 60.05 nM and 89.41 nM in GLP-1R and GIPR cell-based assay respectively **(Fig 1G, 1H)**. The data thus reflects on the potent GLP-1R and GIPR dual agonism of the hybrid peptide I-M-150847 while exhibiting minimal activity towards GCGR. LC/MS analysis, purity, and the secondary structure of the C terminal amidated version of I-M-150847 are provided in **Figure 1 supplementary Fig 1, Figure 1 supplementary Fig 2, and Figure 1supplementary Fig 5.**

GLP-1R and GIPR dual agonist I-M-150847 shows a distinct temporal and spatial signaling and trafficking pattern:

To assess the signaling efficiency in a physiological milieu, we carried out a comparative analysis of I-M-150847 with liraglutide in BRIN-BD11 pancreatic beta cells that express both the receptors **(Fig 2 supplementary Fig 1).** I-M-150847

demonstrated a 30 fold lower potency than liraglutide in cAMP-responsive element luciferase reporter assay **(Fig 2A).** The time-course analysis revealed a distinct temporal pattern of cAMP accumulation upon treatment of BRIN-BD11 pancreatic beta cells with I-M-150847 as compared to liraglutide. In the case of liraglutide, we observed a prolonged cAMP generation that is sustained at 90 min after the treatment with the ligand **(Fig 2B).** In contrast, cAMP accumulation upon I-M-150847 treatment is short-lived as it maximizes at a 10 min time point and recedes abruptly at 30 min following the treatment of cultured pancreatic beta cells with the agonist **(Fig 2C).** Along with the unique temporal dynamics of cAMP accumulation, we observed an altered spatial distribution of GLP-1R- GFP that is characterized by reduced internalization of the activated receptor upon treatment with I-M-150847. As revealed in **Fig 2D,** GLP-1R GFP is distributed at the plasma membrane as well as in the cytoplasm in untreated pancreatic beta cells. Upon treatment with liraglutide for 10 minutes, we observed a complete internalization of GLP-1R-GFP from the plasma membrane to the cytoplasm. A complete loss of the annular cell surface signal of GLP-1R- GFP resulted in the enhancement of the localization of internalized GLP-1R as punctate dots at 10 minutes and 30 minutes following the treatment with liraglutide**.** In contrast, when treated with I-M-150847 for 10 minutes, we observed a drastically reduced internalization of GLP-1R-GFP as a substantial proportion of the receptor remained at the plasma membrane post activation of GLP-1R**.** The data highlights that the localization of GLP-1R-GFP at the plasma membrane following the treatment with I-M-150847 corresponds to the active state of the receptor as measured by its efficiency to generate cAMP second messenger signaling (**Fig 2C**). Collectively, this data illustrates that I-M-150847, unlike

other GLP-1R monoagonists (23, 26), generates a comparatively short-lived cAMP response at the plasma membrane to initiate incretin receptor signaling in pancreatic beta cells.

I-M-150847 promotes glucose-stimulated insulin secretion and improves glycemic control.

The cAMP signaling pathway regulates insulin vesicle exocytosis through PKA and Epac2 dependent pathways (27-29). Intuitively, the specific spatiotemporal distribution of the incretin receptor-ligand complex along with the unique cAMP generation pattern upon I-M-150847 treatment might impact the dynamics of insulin vesicle exocytosis. To explore the hypothesis, we evaluated insulin vesicle fusion using fixed TIRF microscopy at the 10-minute time point post-treatment with liraglutide or I-M-150847 following the method of Bogan et.al (30) and Girada et.al (23). We observed distinct fluorescence spots of insulin-GFP in BRIN-BD11 pancreatic beta cells treated with 0.1mM glucose **(Fig 3A (i))** that increase in size when exposed to 11mM glucose **(Fig 3A (ii)).** The insulin-GFP fluorescent spots increases in number in the presence of 100 nM liraglutide **(Fig 3A (iii)).** However, we observe diffuse clouds of bright Insulin–GFP fluorescence at the TIRF zone upon treatment with 10 μM I-M-150847 **(Fig 3A (iv)).** To evaluate whether this bright Insulin-GFP fluorescence at the TIRF zone represents insulin vesicle secretory bursts as a consequence of the enhanced duration of the opening of the fusion pore, we measured I-M-150847-mediated GSIS in the BRIN-BD11 pancreatic beta cells. As **Fig 3B** reveals, I-M-150847 enhances GSIS in a dose-dependent manner, the increase is comparable to liraglutide at 100nM and 1μM concentration at 30 minutes post-treatment with the agonists despite comparatively reduced cAMP

accumulation upon I-M-150847 treatment. The in vitro efficacy of I-M-150847 is efficiently translated in vivo, as we observed a significant reduction of fasting hyperglycemia in DIO mice after 7days of twice-daily dosing (100nmol /kg bodyweight) with I-M-150847 **(Fig 3C)**. We next evaluated the efficacy of I-M-150847 for blood glucose-lowering upon chronic treatment. As our data shows, the fasting blood sugar in the control group is 157.0±5.373 mg/dL whereas twice-daily dosing with I-M-150847 for a period of 6 weeks reduces the fasting blood glucose to 93.33± 2.871 mg/dL(***$p<0.001$.student's t-test, unpaired) displaying the efficacy of the dual agonist in reducing hyperglycemia upon chronic treatment **(Fig 3D)**. I-M-150847 significantly improves glucose excursions in mice fed on the high-fat diet (reduction from AUC 24045 ± 1584 arbitrary units to AUC 9877 ± 301.6, ***$p< 0.001$, one way ANOVA, Tukey's multiple comparison test) as revealed in intraperitoneal glucose tolerance test (ipGTT) **(Fig 3E).** The data, taken together, demonstrate the potential of I-M-150847 in improving glycemic control in the diet-induced rodent model of diabetes and obesity.

I-M-150847 reduces the food intake and decreases body weight gain in mice fed on the high-fat diet.

We next evaluated the impact of I-M-150847 on the food intake and body-weight gain in the mice fed on the high-fat diet. Treatment with I-M-150847 for the first 6 days of dosing causes a significant reduction in the cumulative food intake from the 3rd day till the 6th day (mean cumulative food intake, *control*: 20.00 ± 1.84 grams, and upon *I-M-150847 treatment*: 14.83 ± 0.98 grams n=6 for each group, $p<0.05$ student's t-test) **(Fig 4A).** The decrease in food intake contributes to a significant reduction in the body weight gain during 7days of I-M-150847 treatment (mean percent body weight gain:

control: 8.588 ± 1.393 % and upon *I-M-150847 treatment*: -2.741 ± 1.209 % n=6 for each group, p<0.001, student's t-test comparing between the groups receiving normal saline or I-M-150847) **(Fig 4B)**.To assess whether the decrease in the body-weight gain is a consequence of the reduction in the food intake, we pair-fed the animals for the next six days **(Fig 4C)**. As **Fig 4D** revealed, upon pair feeding (mean cumulative food intake, *control*: 15.67 ± 1.453 grams, n=6, and upon *I-M-150847 treatment*: 16.67 ± 1.282 grams n=6; p=0.61 *not significant*;), both the control and the I-M-150847 treated group has similar body-weight gain. The data signifies that the diminished energy uptake is the major contributor to the reduction in body weight gain upon treatment with the dual agonist I-M-150847 (mean % body-weight gain, *control*: 1.031 ± 1.272 %, and upon *I-M-150847 treatment*: 0.9540 ± 0.9704%, n=6 for each group, p=0.96 *not significan*t); The animals were then fed ad libitum under continued treatment with I-M-150847 for a period of 4 weeks after which the body weight was measured. As **Fig 4E** shows, I-M-150847 treatment causes a significant decrease in the body weight gain (mean % body-weight gain, *control*: 4.22 ± 1.97 %, n=6, and upon *I-M-150847 treatment*: -9.62 ± 1.508%, n=6, ***p<0.001; student's t-test unpaired). We observed a reduction in mesenteric white adipose tissue (WAT) in I-M-150847 treated mice (mean % normalized fat mass, *control*: 0.2752 ± 0.019% n=5 and upon *I-M-150847 treatment: 0.1250 ± 0.05612 %, n=5*,*p<0.05, student's t-test unpaired) (**Fig 4F**) along with a subtle reduction of epididymal and retroperitoneal WAT **(Figure 4, supplementary Fig 1)**. The data indicate that the reduction of WAT upon I-M-150847 treatment may contribute to the maintenance of lower body weight that we observe during chronic treatment of DIO mice with the GLP-1R-GIPR dual agonist.

Discussion:

Multi-receptor agonism of incretins has recently emerged as a preferred therapy to achieve superior glycemic control and reduction of obesity (31, 32). The concept of unimolecular GLP-1R and GIPR dual agonism first described by Finan et.al revealed the efficiency of hybrid peptides in reducing diabesity more effectively than the conventional GLP-1R agonists (10). Consistent with these findings, the dual GLP-1R and GIPR agonist Tirzepatide (LY3298176) developed by Eli Lilly showed better efficacy than the most potent GLP-1R agonist semaglutide in reducing HbA1c, body weight, and serum triglycerides in SURPASS phase 3 clinical trials (33-37). Tirzepatide and the related class of dual GLP-1R and GIPR agonists thus offer the promise to achieve superior long-term glycemic control with a significant reduction of obesity (38, 39).

The majority of the unimolecular incretin dual agonists reported to date were designed by intermixing GLP-1 and GIP amino acids in a single peptide using either glucagon (10), oxyntomodulin ((17, 18),(25), (40), or GIP as the base peptide (41). The incretin receptor dual agonist I-M-150847 was designed following a completely different approach. Here the emphasis was given on the two-domain activation model for the Class B GPCRs (42). The model proposes that the interaction between the C- terminal domain of the ligand with the extracellular domain (ECD) of the receptor supports the engagement of the N-terminal domain of the ligand with the central transmembrane domain of the receptor, causing a conformational rearrangement that initiates the second messenger signaling (19, 21, 42). Consequently, the data on the crystal structure of GLP-1, exendin-4, and GIP bound to respective GLP-1R and GIPR ECD

(19-21) provided us the critical insights for the designing of the middle and the C terminal region of the hybrid agonist that binds with the incretin receptor ECD. We focused on the Lys 30 of GIP that aligns with the corresponding amino acid residue of oxyntomodulin and experimentally determined the activity by cAMP reporter assays. We replaced the tryptophan cage (Trp-cage) at the C terminus of exendin-4 (21, 43-45) despite its presence in Tirzepatide (Kegg Drug D11360) and stapled GLP-1R dual agonist O14(25) as previous studies reported the redundancy of the motif for the preservation of high binding affinity for GLP-1R (45).

We initiated our experimental analysis by synthesizing I-M-150845 (**Table 1, Figure 1Supplementary Fig 3**) upon addition of GLP-1 and GIP-specific amino acids to the first 9 amino acid residues of the peptide IM150844 that corresponds to the N-terminal sequence of exendin-4. I-M-150845 showed dual GLP-1R and GIPR activity in cAMP reporter assays (**Table 1**). From the structural perspective, the amino acid residues Phe^{22}, Val^{23}, Leu^{26}, and Leu^{27} of the amphipathic alpha-helix of GIP that forms hydrophobic interactions with GIPR ECD is present in the hybrid peptide I-M-150845. In addition, we retained Asp^{15}, Gln^{19}, Gln^{20}, Leu^{26}, and leu^{27}, the amino acids that form an extensive hydrogen-bonding network with several residues of GIPR ECD in I-M-150845 to provide GIPR-specific activity. In contrast, the amino acids of the exendin-4/GLP-1 amphipathic alpha-helix that support the hydrophilic interactions with GLP-1R ECD are absent in I-M-150845. Of the 7 amino acids of exendin-4, Ala^{18}, Val^{19}, Phe^{22}, Ile^{23}, Trp^{25}, Leu^{26}, and Pro^{31} that form hydrophobic interaction with GLP-1R ECD, only Phe^{22} and Leu^{26} are retained in hybrid dual agonist I-M-150845. We hypothesized that Val^{27} at the I-M-150845 has a compensatory influence as it establishes hydrophobic contact as

well as hydrogen bonding with GLP-1R ECD in the receptor-ligand crystal complex (20). To experimentally ascertain the importance of Val^{27} for GLP1R specific activity, we synthesized a new incretin agonist I-M-150846 where the C- terminal amino acids Val^{27}-Gly^{31} of I-M-150845 are substituted with 11- amino acid C terminus (Met^{27}-Ala^{37}) of oxyntomodulin (**Figure1 supplementary Fig 4**). The substitution removes Val^{27} but introduces Lys^{30} which in GIP establishes an intricate hydrogen-bonding network with several residues in the C terminal part of GIPR ECD (19). The incretin agonist I-M-150846 revealed a complete loss of function at GLP-1R while retaining GIPR activity **(Table 1).** We then replaced GIP- specific Tyr^{10}-Asn^{24} of I-M-150846 with amino acid residues Leu^{10}- Glu^{24} of exendin-4 (**Figure1 supplementary Fig 5**) that forms superior helical architecture with GLP-1R ECD (21). The resultant incretin agonist I-M-150847 showed robust GLP-1R and GIPR dual agonism signifying that in the absence of Trp cage, the presence of the amino acid residues Leu^{10}- Glu^{24} of exendin-4 in the hybrid agonist peptide is critical to establish a stable interaction with the GLP-1R ECD thereby restoring the functional activity towards GLP-1R as measured by cAMP reporter assay. The data also implies that Phe^{22}, Leu^{26}, and Lys^{30} are the crucial amino acids that confer binding to the GIPR ECD required for the GIPR-specific activity of I-M-150847. The dual agonist I-M-150847 revealed unique trafficking and activation pattern as compared to sustained cAMP generation by GLP-1R monoagonists (23, 26). The majority of GLP-1R agonists, with a notable exception with exendin F1 ((46, 47), contribute to sustained cAMP generation from endosomes following internalization of the receptor-ligand complex (22, 23). We first reported that the internalization of GLP-1 is compromised in the presence of GIPR full agonist IUB68 (22). Consistent with our

observation, the dual agonist Tirzepatide revealed reduced internalization upon binding to the receptor, the phenomenon is attributed to its limited ability to recruit beta-arrestin (41). Similar to Tirzepatide, we observed reduced internalization of the GLP-1 receptor upon activation with I-M-150847. More importantly, unlike other GLP-1R monoagonists (22, 23, 26), I-M-150847- mediated incretin receptor activation is short-lived as it coincides with the spatial location of the activated receptor at the plasma membrane. The functional implication of this unique spatio-temporal trafficking and signaling is yet unclear. In the case of I-M-150847, despite reduced cAMP generation, GSIS is comparable to liraglutide. We observed diffuse clouds of bright Insulin-GFP fluorescence at the TIRF zone upon treatment with I-M-150847 implying enhanced duration of the opening of the fusion pore facilitating insulin vesicle exocytosis **(Fig 3A).** The data highlights the significance of the spatial cAMP generation in mediating SNARE assembly to promote insulin vesicle fusion to the plasma membrane which deserves attention in future research.

The efficiency of I-M-150847 in enhancing GSIS is translated to the improvement of glucose tolerance in DIO mice upon chronic treatment as measured by ipGTT. The glucose excursion in DIO mice, which is significantly improved after 4-week twice-daily treatment with I-M-150847 amide was found to be superior to mice fed on the chow diet. However, whether I-M-150847 enhances insulin sensitivity is yet unexplored which is a limitation of the present study.

The improved weight loss response that we observed on the short-term treatment of I-M-150847 is a consequence of reduced food intake as evidenced from the pair-fed studies. However, the mechanism of the I-M-150847-mediated regulation of the gut-

brain axis is presently unexplored. Reduced gastric emptying and delayed intestinal motility have been reported in the case of long-acting GLP-1R agonists(48) as well as GLP-1R GIPR dual agonist Tirzepatide(49).GIPR is present in key feeding centers at the hypothalamus and intracerebroventricular administration of acyl GIP causes acute neural activation in the feeding centers that includes the arcuate nucleus, dorsomedial hypothalamic nucleus, ventromedial nucleus of the hypothalamus, and lateral hypothalamus (50). Future research is needed to explore whether I-M-150847 causes similar neural activity in the feeding centers to trigger early induction of satiety. Collectively, the preclinical data presented in this study demonstrate I-M-150847 as a novel GLP-1R and GIPR dual agonist with the potent insulinotropic activity in rodents that improves glycemic control. The mechanism of action, though incompletely understood, is unique as compared to our previous report on GLP-1R mediated signaling in pancreatic beta cells. Further, I-M-150847 exhibited a significant reduction of food intake, loss of body weight, and reduction of mesenteric adipose mass that highlights the therapeutic potential of the novel hybrid agonist in ameliorating type2 Diabetes and obesity.

Figure Legends:

Fig 1: Discovery of I-M-150847 a GLP-1R, GIPR dual Incretin Receptor agonist.

A. Screening of incretin agonists in cell-based human GLP-1R, cAMP-responsive element luciferase reporter assay. Y-axis represents relative Luciferase units normalized by β-galactosidase expression. The data expressed as fold over the basal is presented as means ± SD. Lira: Liraglutide; Oxm: Oxyntomodulin, EX-4: Exendin-4.

B. Screening of incretin agonists in cell-based human GIPR, cAMP-responsive element luciferase reporter assay. Y-axis represents relative Luciferase units normalized by β-galactosidase expression. The data expressed as fold-over basal is presented as means ± SD. Lira: Liraglutide; Oxm: Oxyntomodulin, EX-4: Exendin-4.

C. Screening of incretin agonists in cell-based human GCGR, cAMP-responsive element luciferase reporter assay. Y-axis represents relative Luciferase units normalized by β-galactosidase expression. The data expressed as fold-over basal is presented as means ± SD. Lira: Liraglutide; Oxm: Oxyntomodulin, EX-4: Exendin-4.

D. Dose-dependent assessment of the efficacy of I-M-150847 in human GLP-1R, cAMP-responsive element luciferase reporter assay. The data is represented as mean ± SEM of three independent experiments. *$p<0.05$ determined by Student's t-test comparing cAMP generation by IM-150847 (1μM) with Exendin-

4(1μM) as measured by cyclic AMP responsive element luciferase assay; ns= not significant. Lira: Liraglutide; Oxm: Oxyntomodulin, EX-4: Exendin-4.

E. Dose-dependent assessment of the efficacy of I-M-150847 in human GIPR, cAMP-responsive element luciferase reporter assay. The data is represented as mean ±SEM of three independent experiments. ***$p<0.001$ determined by Student's t-test comparing cAMP generation by IUB68 (10μM) with other incretin agonists. ns= not significant. Lira: Liraglutide; Oxm: Oxyntomodulin,

F. Dose-dependent assessment of the efficacy of I-M-150847 in human GCGR cAMP-responsive element luciferase reporter assay. The data is represented as mean ±SEM of three independent experiments.

G. Dose-response curve for stimulation of cAMP generation as measured by cAMP-responsive element luciferase reporter assay.EC_{50} values represent the effective peptide concentrations (nM) that stimulate the half-maximum activation at the GLP-1R. The data is represented as mean ±SEM of four independent experiments.

H. Dose-response curve for stimulation of cAMP generation as measured by cAMP-responsive element luciferase reporter assay.EC_{50} values represent the effective peptide concentrations (nM) that stimulate the half-maximum activation at the GIPR. The data is represented as mean ±SEM of four independent experiments.

Figure 1 supplementary Fig 1:

LC-MS analysis of peptide I-M-150847 amide.

Figure1supplementary Fig 2:

RP-HPLC of peptide I-M-150847 amide.

Figure 1supplementary Fig 3:

Design of the peptide I-M-150845

A. Amino acid constituents of peptide I-M-150845. The amino acids common to exendin-4, GLP-1, and GIP are colored black, green, and red respectively.
B. Cartoon of the predicted secondary structure of I-M-150847 as modeled by Swiss- model protein structure homology modeling server. C=loop or irregular, H=α helix, T= Hydrogen bonded turns.
C. Ramachandran plot for I-M-150845 using Mol Probity version 4.4 in Swiss-model protein structure homology modeling server.

Figure 1 supplementary Fig 4:

Design of the peptide I-M-150846

A. Amino acid constituents of peptide I-M-150846. The amino acids common to exendin-4, GIP, and oxyntomodulin are colored black, red, and blue respectively.
B. Cartoon of the predicted secondary structure of I-M-150846 as modeled by Swiss- model protein structure homology modeling server. C=loop or irregular, H=α helix, T= Hydrogen bonded turns.
C. Ramachandran plot for I-M-150846 using Mol Probity version 4.4

Fig 1 Supplementary Fig 5:

Physical Characterizations of peptide I-M-150847.

A. Amino acid constituents of I-M-150847. The amino acids common to exendin-4, GIP, and oxyntomodulin are colored black, red, and blue respectively
B. Cartoon of the predicted secondary structure of I-M-150847 as modeled by Swiss- model protein structure homology modeling server. C=loop or irregular, H=α helix, T= Hydrogen bonded turns. G= 3-helix (3_{10}- helix), S= bend.
C. CD analysis of I-M-150847.
D. Ramachandran plot for I-M-150847 using Mol Probity version 4.4

Figure 2: I-M-150847 mediated signaling and trafficking in cultured pancreatic beta cells.

A. Concentration-response curves of I-M-150847 vis-à-vis liraglutide for cAMP accumulation as measured by cAMP-responsive element luciferase reporter assay. EC_{50} values represent the effective peptide concentrations (nM) of liraglutide and I-M-150847 that stimulate the half-maximum activation. The data is represented as mean ±SEM of three independent experiments.
B. The time-course of I-M-150847–mediated cAMP accumulation in BRIN-BD11 pancreatic beta cells. The cells were incubated with I-M-150847(10μM) and 3 minutes after the incubation the excess ligand was washed with KRB buffer. The cAMP was measured at less than 1 minute, 5, 10, 15, 30, and 60 min after KRB wash using Direct cAMP Enzyme Immunoassay. The data are expressed as mean ±SEM of four independent experiments. ** $p< 0.01$ comparing cAMP generation upon I-M-150847 treatment at 5min versus 1 min. ***$p<0.001$

comparing cAMP generation upon I-M-150847 treatment at 5 min versus 30 min (one-way ANOVA Tukey's multiple comparison test).

C. The time-course of liraglutide–mediated cAMP accumulation in BRIN-BD11 pancreatic beta cells. The cells were incubated with liraglutide (100nM) and 3 minutes after the incubation the excess ligand was washed with KRB buffer. The cAMP was measured at 5, 15, 30, and 90 min after KRB wash using the direct cAMP enzyme immunoassay. The data are expressed as mean ±SEM of three independent experiments. ns =non-significant (one-way ANOVA Tukey's multiple comparison test).

D. The GLP-1R GFP trafficking in pancreatic beta cells upon activation by I-M-150847 (1μM) or liraglutide (100nM). BRIN-BD11 pancreatic beta cells were transfected with GLP-1R-GFP and stimulated with agonists for different time intervals. They were then fixed and visualized by confocal microscopy. White arrows point at the location of the activated GLP-1R. Images were representative of three independent experiments.

Figure 2 Supplementary Fig 1:

Relative mRNA expression of GLP-1R and GIPR in BRIN-BD11 pancreatic beta cells. ***$p<0.001$ comparing GLP-1R and GIPR expression.

Figure 3: I-M-150847 promotes GSIS and enhances insulinotropic response

A. TIRFM on fixed BRIN-BD11 pancreatic beta cells assessing the insulin vesicle exocytosis in the presence of 0.1mM glucose(i) or 11 mM glucose (ii) and in the presence of 100 nM liraglutide (iii) and 10μM I-M150847 (iv). Dots and clouds of

fluorescence are marked by arrows. Images are representative of 3 independent experiments (n=15 cells for each experiment). The grey arrows point at the insulin-GFP at the TIRF zone as dots or as the clouds of fluorescence.

B. Effect of I-M-150847 or liraglutide on GSIS in BRIN-BD11 pancreatic beta cells. Data represent means ± SEM of three independent experiments. ***$p<0.001$ determined by one-way ANOVA ((Tukey's multiple comparison tests) evaluating GSIS upon I-M-150847 or liraglutide treatment at different concentrations as compared to treatment with 16.7 mM glucose.

C. Impact of I-M-150847 (twice-daily dosing) on fasting blood sugar of C57BL/6 DIO mice after 7-day treatment. Data represent means ± SEM (n=6) *$p<0.05$ determined by one-way ANOVA (Tukey's multiple comparison tests) comparing fasting blood sugar between vehicle and 0 day and 7th day of I-M-150847 treatment.

D. Impact of I-M-150847 (twice-daily dosing) on fasting blood sugar of C57BL/6 DIO mice after 4 weeks of treatment. Data represent means ± SEM (n=6),***$p<0.001$ determined by Student's t-test comparing fasting blood sugar between the group treated with vehicle and I-M-150847.

E. Intraperitoneal glucose tolerance test (ipGTT) in C57BL/6 male mice fed on the chow diet, high-fat diet, and the diet-induced obese (DIO) mice receiving subcutaneous injections of I-M-150847 (twice-daily dosing) for a period of 6 weeks. *Inset.* The Area under the Curve (AUC) of the IPGTT in mice fed on chow diet, high-fat diet, and DIO mice receiving subcutaneous injections of I-M-150847. Data represent means ± SEM (n=6), ***$p<0.001$ determined by one-way

ANOVA (Tukey's multiple comparison tests) comparing glucose excursions between chow diet-fed mice, DIO mice, and DIO mice treated with I-M-150847.

Figure 4: I-M-150847 reduces the food intake and decreases body weight gain in DIO mice.

A. Cumulative food intake during the first week of I-M-150847 treatment. Data are expressed as means ± SEM (n=6), *p<0.05, **p<0.01 determined by two-way ANOVA, Bonferroni posttests comparing vehicle to I-M-150847 treatment every day for the period of 6 days.
B. Effect on the body weight gain during the first week of I-M-150847 treatment. Data are expressed as means ± SEM (n=6), *p<0.05, **p<0.01, ***p<0.001, determined by two-way ANOVA, Bonferroni posttests comparing vehicle to I-M-150847 treatment every day for the period of 7 days.
C. Cumulative food intake upon treatment with vehicle or I-M-150847 treatment upon pair-feeding. Data are expressed as means ± SEM (n=6)
D. Effect on the body weight gain upon pair feeding during the second week of I-M-150847 treatment. Data are expressed as means ± SEM (n=6)
E. Effect of I-M-150847 on body weight after 4 weeks of treatment on ad libitum – fed DIO mice. Data are expressed as means ± SEM (n=6) ***p<0.001 determined by Student’s t-test comparing vehicle to I-M-150847 treatment.

F. Effect of I-M-150847 on mesenteric WAT after 6 weeks treatment of DIO mice. Data are expressed as means ± SEM (n=5) *p<0.05 determined by Student's t-test comparing vehicle to I-M-150847 treatment.

Fig 4 Supplementary Fig 1:

Effect of I-M-150847 treatment on (a) epididymal WAT and (b) retroperitoneal WAT after 6 weeks of treatment of DIO mice. Data are expressed as means ± SEM (n=6) ns= statistically non-significant.

Materials & Methods:

Materials: Following reagents are used in this study.

REAGENT	SOURCE	IDENTIFIER
CHEMICALS, PEPTIDES AND RECOMBINANT PROTEINS		
RPMI 1640 HiGlutaXL	Himedia	AL-060G
DMEM HIGH GLUCOSE	Himedia	AL-219A
FBS Heat Inactivated(US ORIGIN)	Himedia	RM-10409
TRYPSIN EDTA (10X)	Himedia	TCL-034
Penicillin Streptomycin solution (100X)	Himedia	A001
Gentamycin	Himedia	A005
DMSO	SIGMA	M81802
LIPOFECTAMINE 3000	THERMO	L3000001
IBMX	SANTA CRUZ	SC-201188
GLUCOSE	SIGMA	G-8270
PHOSPHATE BUFFER SALINE	INVITROGEN	70011044
BETA MERCAPTOETHANOL	SIGMA	M6250
RNAiso Plus	Takara	9108
BOVINE SERUM ALBUMIN	SIGMA	A2153
FAT FREE BSA (FRACTION V)	SIGMA	5479
STEADYLITE Plus	PERKIN ELMER	6066751

ATP	SIGMA	A7699
PROTEASE INHIBITOR COCKTAIL	CALBIOCHEM	539131
LIRAGLUTIDE (VICTOZA)	NOVO NORDISK	Acylated GLP-1R agonist
PHOSPHATASE INHIBITOR	CALBIOCHEM	524625
RNA Later solution	AMBION	AM7020
Triton-X 100	SIGMA	T8787
Dr. Trust Glucometer and strips	Dr. Trust USA	9001
IN-M-150845	Designed in-house, synthesized and, purified by GL BIOCHEM, CHINA	Procured through Biotech Desk India
IN-M-150846		
IN-M-150847		
Exendin-4	Prof. Richard DiMarchi's laboratory Indiana University	
Oxyntomodulin	Tocris	2094
IUB-68	Prof. Richard DiMarchi	Indiana University, Bloomington
2-nitro-phenyl beta galactopyranoside	SIGMA	N1127
Paraformaldehyde	SIGMA	158127
Vectashield	Vector Labs	H-1200-10
Plasmid GLP-1R GFP	Mitra Lab	Kuna et.al
Plasmid CRE Luciferase	Richard Day, Indiana University	Kuna et.al 2013(22)
Plasmid GIPR	Bernard Thorens	ADDGENE#14942(51)
Plasmid GCGR	Brian Finan	Novo Nordisk

CRITICAL COMMERCIAL ASSAYS		
BCA PROTEIN ASSAY KIT	SANTA CRUZ	sc-200629
INSULIN ELISA KIT (RAT/MOUSE)	MERCK	EZRMI-13K
cAMP ELISA kit	ENZO	ADI-900-067
TB Green® Premix Ex Taq™ II	Takara	RR820B
PRIMESCRIPT cDNA synthesis kit	Takara	RR014B
PLASMID ISOLATION KIT	INVITROGEN	K210005

OLIGONUCLEOTIDES	
RT-qPCR Primers	IDT

EXPERIMENTAL MODELS/ CELL LINES		
BRIN-BD11 CELL LINE	ECACC	10033003
HEK-293T CELL LINE	ATCC	CRL-3216
C57BL/6J MICE	**Jeeva Life Sciences, Hyderabad**	JLS-000664
Animal Feed (HIGH FAT DIET/CHOW DIET)	**NIN, Hyderabad**	

Methods:

Peptide Synthesis:

Synthesis of the 11- amino acid residue peptide I-M-150844 was carried out in Biotage Syro I automated peptide synthesizer using Wang resin and following Fmoc chemistry. The amino acid that was first loaded to the resin is Phenylalanine and following installation, the capping of residual functional groups on the resin was carried out by treatment with 33% acetic anhydride and pyridine. Before loading of next amino acid, the Fmoc group of the amino acid was deprotected through treatment by 40% piperidine / DMF and the incorporation of the next amino acid was carried out using coupling reagent HBTU (0.5 mmol) and DIPEA/NMP (2 mmol). The peptide was cleaved from the resin by mixing it with TFA/H_2O/TIPS (95:2.5:2.5, 4 ml) and TFA was removed by evaporation on a rotatory evaporator. The crude mixture was triturated (diethyl ether) and purified by preparative HPLC using Agilent column ZORBAX 300SB-C18 (5 µm, 9.4*250 mm).

The other peptides I-M-150845, I-M-150846, and I-M-150847 were designed in-house, outsourced for chemical synthesis and purification to GL Biochem China. The C

terminal amidated version of I-M-150847 was synthesized by Aurigene Pharmaceutical Services, India.

Circular dichroism spectroscopy:

Determination of the secondary structure of I-M-150847 was carried out by using Circular Dichroism Instrument (JASCO, J1500, Easton MD) (52, 53). The spectra from 200 to 260 nm were taken with a data interval of 0.5nm. A bandwidth of 1.00nm with a 100nm/min scanning rate was used to determine the property.10μM of I-M-150847 was used for the study and 50mM Phosphate buffer serves as the blank background. The data were represented as Ellipticity (mdeg) vs wavelength (nm) at Y and X-axis respectively.

Cell Culture:

Pancreatic beta cells, BRIN-BD11 (cat no.10033003) were procured from the European Collection of Authenticated Cell Cultures. The cells were cultured in RPMI media 1640 HiGlutaXL with 10% heat-inactivated fetal bovine serum supplemented with 1mM sodium pyruvate, 50mM β-mercaptoethanol,10mg/mL gentamycin, 100U/mL penicillin, and 100mg/mL streptomycin at an incubation temperature of 37º C with 5% CO_2 following the method of Kuna et. al (22). Human Embryonic Kidney cell lineage (HEK 293T) cells were procured from ATCC (CRL3216). The cells were cultured in DMEM-Hi Glucose media supplemented with 10% heat-inactivated FBS, 10mg/mL gentamycin,

100U/mL penicillin, and 100mg/mL streptomycin at an incubation temperature of 37º C with 5% CO_2, cultured following the protocol recommended by ATCC.

GLP-1R, GIPR, GCGR activation:

Each peptide was tested for its ability to activate GLP-1R, GIPR, or GCGR in a cell-based cAMP-responsive element luciferase reporter assay following the method of Kuna et.al (22). Briefly, HEK 293T cells were cultured in a 60mm tissue culture treated dish. Upon 70% confluency, the cells were transiently transfected with cAMP-responsive element luciferase reporter plasmid, beta-galactosidase plasmid, and GIP-R or GLP-1 R, or GCGR plasmid in a 3:1:3 ratio. The transient transfection was carried out using lipofectamine 3000 following the manufacturer's protocol. After 4 hours of transfection, the cells were seeded in a tissue culture grade 96 well plate at a density of 50000 cells / well. After overnight incubation, the cells were treated with different concentrations of agonists for the different cell-based assays. After 4 hours of treatment, the media was aspirated and cells were lysed and the luminescence was measured using Steady lite Plus reagent (Perkin Elmer Life and Analytical Science, Waltham, MA)after 15 minutes of shaking at 300 rpm at room temperature in dark. 2-nitro-phenyl beta galactopyranoside (Sigma) was used to carry out a beta-galactosidase assay for correcting the inter-well transfection variability.

cAMP accumulation in pancreatic beta cells:

The accumulation of cAMP was measured in cultured BRIN-BD11 at different time points upon agonist treatment. 10µM I-M-150847 and 100nM of Liraglutide were tested

for the time-course of cAMP generation using a direct cAMP ELISA kit (Enzo Life Sciences, Cat. No. ADI-900-163). The assay was carried out following the protocol of Girada et. al (23) with modifications. Briefly, BRIN-BD11 cells were seeded in 24 well-treated plates at a density of 0.1 million cells/well. After overnight incubation, the cells were treated with 10µM I-M-150847 or 100nM of Liraglutide along with 200µM IBMX in KRB-BSA medium for different time points. The cells treated with incretin receptor agonists were incubated for 3 minutes and then the treatment medium was washed off and replaced with KRB-BSA medium with 200µM IBMX and incubated for 1, 5,10,15,30, and 60 minutes after which the cells were lysed and processed for the cAMP ELISA assay. Protein quantification was carried out using BCA following kit protocol.

GLP-1R internalization assay:

Assessment of GLP-1R internalization was carried out in BRIN-BD11 pancreatic beta cells and monitored using confocal microscopy. The cells were transfected with GLP-1R-GFP using lipofectamine 3000 and seeded in six-well plates on 22*22mm sterile cover glass coated with poly-L-lysine. 48-hours after transfection, the cells were washed with sterile PBS and incubated with I-M-150847 (1µM) or liraglutide (100nM) in 200µL of Krebs-HEPES buffer for 60 min at 4 °C in a humidified chamber in the dark. Cells were then washed in PBS and incubated at 37° C for 1 min, 10 minutes, and 30 minutes after which they are fixed in 4% paraformaldehyde and imaged using a Zeiss LSM 710 confocal laser scanning microscope (Carl Zeiss, Oberkochen, Germany) equipped with krypton-argon laser sources. Pinhole diameter was maintained at 1 airy unit. Fields

were selected using 20X objective and image acquisition was carried out using a 63× oil immersion objective lens.

Insulin vesicle exocytosis:

Insulin vesicle exocytosis was assessed using total internal reflection fluorescence microscopy (TIRFM) in fixed BRIN-BD11 pancreatic beta cells following the method of Girada et.al (23). The cells were seeded on sterile poly-L-lysine coated cover glass at a density of 200,000 cells per well in a 6-well plate and transfected with Insulin-GFP using lipofectamine 3000. 48 hours after transfection, the cells were incubated with incretin agonists for 1h at 4°C. The cells were then exposed to 0.1mM glucose or 11mM glucose for 10 min in Krebs-Ringer Buffer containing 0.1% Fat-free BSA in the presence of I-M-150847 or liraglutide and further fixed with 3% paraformaldehyde. For TIRFM, the cover-glasses were mounted on a custom-made holder with 500µL of 100nM phosphate buffer pH 7.2. The cells were visualized through a custom-built TIRF microscope equipped with an EM-CCD camera, a 100×oil-immersion objective (Nikon), high NA (NA = 1.49), and 450-nm diode laser. The distance, exposure, evanescent field (100nm) was adjusted with THOR Labs-Kinesis software, and image analysis was carried out using ImageJ.

Insulin secretion:

Insulin secretion was assessed using Millipore rat/ mouse insulin ELISA kit (Merck, EZRMI-13K) following the method of Asalla et.al.(54) Briefly, BRIN-BD11 cells were seeded in 24 well tissue culture plates at a density of 100000cells / well. In the next day, the cells were treated with Kreb's Ringer Bicarbonate buffer (KRB) [115 mM NaCl, 4.7 mM KCl, 1.28 mM $CaCl_2$, 1.2 mM KH_2PO_4, 1.2 mM $MgSO_4$, 10 mM $NaHCO_3$, 0.1% (wt./vol) BSA, pH 7.4] for 1h without glucose. Glucose stimulated insulin release was assessed in the presence of indicated concentrations of glucose and incretin receptor agonists for 30 min and the supernatant was collected, centrifuged, and processed for the ELISA as per the manufacturer's protocol. The cells were lysed with 0.1% Triton-X 100 and processed for protein quantification to normalize the insulin secretion. The data were expressed as fold-over basal insulin secretion (ng insulin/µg protein).

Total RNA isolation, cDNA preparation, and qRT PCR

The RNA extraction was carried out by phenol-chloroform extraction protocol from cultured BRIN-BD11 pancreatic beta cells.1 µg of total RNA was used for first-strand cDNA synthesis. Takara Prime script cDNA synthesis kit was used to carry out the two-step cDNA synthesis following the manufacturer's protocol. The mRNA for GLP-1R and GIPR was amplified and quantified by quantitative real-time PCR by using Quant Studio 5 (A&B Biosystems). 2XSYBR master mix (Takara Life Sciences) reagent was used for the assessment of the relative abundance of mRNAs measured using the $2^{-\Delta\Delta CT}$ method (Livak and Schmittgen, 2001) (55). Normalization was done by using GAPDH as an invariant reference. Primers used for amplification are as follows: GLP1R *f*:

TATTGGCTCATCATACGCTTG; GLP1R*r:* GTCTGCATTTGATGTCGGTCT; GIPR *f*: CGAAGTCAAAGCCATTTGGT; GIPR *r*: CCAGCCTTAGTCGGTAGTCG; GAPDH *f*: AGTTCAACGGCACAGTCAAG; GAPDH *r*: TACTCAGCACCAGCATCACC.

Animal Experiments:

Animal experiments were performed following the guidelines of Control and Supervision of Experiments on Animals (CPCSEA) upon permission from the Institutional Ethical Committee Hyderabad, India (UH/IAEC/KS/2021-1/36) and the National Institute of Nutrition, Hyderabad, India (P23F/IAEC/NIN/11/2017/PM/C57BL6/J-260(M)). C57BL/6 male mice of 5 weeks of age were procured from Jeeva Life Sciences, Hyderabad (Cat No: JLS-000664). Only male mice were used for the study since female mice are mostly protected from diet-induced obesity (56).

The mice were group-housed or single-housed on a 12:12 h light-dark cycle at 22˚-24˚C and were fed ad-libitum on a diabetogenic diet (6) which is a high-sucrose diet with 58% kcal from fat for 8 weeks before the initiation of the pharmacological studies. The drug treatment was carried out with I-M-150847amidated at the C terminal.

a. <u>Glucose tolerance test:</u>

In the 13th week, mice were randomized and subjected to pharmacological dosing (six mice/group). The animals were grouped into three groups: a) HFD control group, b) HFD peptide treatment group, and c) Chow-fed control group. The HFD control group was administered a subcutaneous injection of vehicle (0.9% normal saline), or I-M-150847 (100 nmol /kg body weight) twice daily for a period of 6 weeks. For determination of glucose tolerance, DIO mice were

subjected to 5h of fasting following which intraperitoneal injection of glucose (2 g/kg body weight) (D-glucose [Sigma] 20% w/v in 0.9% normal saline) was administered. Glucose levels from tail vein blood were measured with a handheld glucometer (Dr. Trust glucometer) before (0 min) and at 15, 30, 60 90, and 120 minutes after the glucose challenge.

b. Bodyweight, food intake, and measurement of visceral adipose mass

For the measurement of cumulative food intake vis-a`-vis body weight gain, C57BL/6 male mice (6 mice/group) fed on the high-fat diet were treated with the subcutaneous injection of I-M-150847 (100nmol/kg) twice daily or vehicle and fed ad libitum for a period of 7 days, and the body-weight gain and cumulative food intake was measured every day for the first 7 days. In the second week, the subcutaneous injection of I-M-150847 (100nmol/kg) twice daily was continued but the control and treated mice were pair-fed for the entire second week and the body-weight gain and cumulative food intake was measured every day. At the end of the second week, the animals were fed ad libitum and subcutaneous injection of I-M-150847 (100nmol/kg) twice daily was continued for another 4 weeks following which bodyweight was measured.

For the measurement of visceral WAT, animals were sacrificed at the end of the experiment, and retroperitoneal, mesenteric, and epididymal fat pads along with the blood samples were collected from individual animals and stored at -80°C for further processing.

Statistical analysis:

Statistical analyses were performed with GraphPad Prism 6.0 and presented as means ± SEM. The analysis of the experiments was performed with one-way ANOVA (Tukey's multiple comparison test) and Student's t-test or two-way ANOVA Bonferroni posttests *P* values lower than 0.05 were considered significant.

Ethics:

The animal studies were carried out following the guidelines of Control and Supervision of Experiments on Animals (CPCSEA) upon permission from the Institutional Ethical Committee Hyderabad, India (UH/IAEC/KS/2021-1/36) and the National Institute of Nutrition, Hyderabad, India (P23F/IAEC/NIN/11/2017/PM/C57BL6/J-260(M).

Author Contributions:

SB, RB, and JE were responsible for conducting experiments, data collection, and analysis. SK, TD, and AI provided the necessary support for conducting experiments. RB and SB carried out TIRFM with the help of PM, KG, and SD. NC and VR synthesized some of the peptides and carried out physical characterizations. RB, SB, and PM carried out the in silico analysis of the structure of novel incretin peptides. PM conceptualized the project and supervised the experiments, designed the peptides, analyzed and interpreted the data, wrote the manuscript upon discussion with RB and SB, and take the responsibility for the integrity and accuracy of the data. All authors have full access to the data related to the manuscript and approved the final version of the manuscript for publication.

Acknowledgments:

The work has been supported by Department of Science and Technology Grants; EMR/2016/007057 provided to PM, VR, and AI. Fellowship of RB and SB is supported by Council of Scientific and Industrial Research (CSIR No: 09/0985 (0032)/2019-EMRI) and ICMR senior research fellowship (No 2017-3891-CMB/BMS). SB and RB are registered at Manipal Academy of Higher Education (MAHE) for their doctoral degree. IUB68 and Exendin-4 are generous gifts from Richard DiMarchi Laboratory, Indiana University, pcDNA3-GCGR is a gift from Brian Finan, Novo Nordisk.

Declaration of interest:

Authors declare no conflicts of interest.

References:

1. D. J. Drucker, The biology of incretin hormones. *Cell Metab* **3**, 153-165 (2006).
2. L. R. Ranganath, The entero-insular axis: implications for human metabolism. *Clin Chem Lab Med* **46**, 43-56 (2008).
3. R. E. Amori, J. Lau, A. G. Pittas, Efficacy and safety of incretin therapy in type 2 diabetes: systematic review and meta-analysis. *JAMA* **298**, 194-206 (2007).
4. A. Astrup *et al.*, Effects of liraglutide in the treatment of obesity: a randomised, double-blind, placebo-controlled study. *Lancet* **374**, 1606-1616 (2009).
5. A. Andersen, A. Lund, F. K. Knop, T. Vilsboll, Glucagon-like peptide 1 in health and disease. *Nat Rev Endocrinol* **14**, 390-403 (2018).
6. S. Bele *et al.*, MS-275, a class 1 histone deacetylase inhibitor augments glucagon-like peptide-1 receptor agonism to improve glycemic control and reduce obesity in diet-induced obese mice. *Elife* **9** (2020).
7. M. A. Nauck *et al.*, Preserved incretin activity of glucagon-like peptide 1 [7-36 amide] but not of synthetic human gastric inhibitory polypeptide in patients with type-2 diabetes mellitus. *J Clin Invest* **91**, 301-307 (1993).
8. J. J. Holst, Implementation of GLP-1 based therapy of type 2 diabetes mellitus using DPP-IV inhibitors. *Adv Exp Med Biol* **524**, 263-279 (2003).
9. M. Bastin, F. Andreelli, Dual GIP-GLP1-Receptor Agonists In The Treatment Of Type 2 Diabetes: A Short Review On Emerging Data And Therapeutic Potential. *Diabetes Metab Syndr Obes* **12**, 1973-1985 (2019).
10. B. Finan *et al.*, Unimolecular dual incretins maximize metabolic benefits in rodents, monkeys, and humans. *Sci Transl Med* **5**, 209ra151 (2013).
11. R. D. DiMarchi, "Let's Stay Together"; GIP and GLP-1 dual agonism in the treatment of metabolic disease. *Mol Metab* **18**, 1-2 (2018).
12. T. Coskun *et al.*, LY3298176, a novel dual GIP and GLP-1 receptor agonist for the treatment of type 2 diabetes mellitus: From discovery to clinical proof of concept. *Mol Metab* **18**, 3-14 (2018).
13. J. P. Frias *et al.*, Efficacy and safety of LY3298176, a novel dual GIP and GLP-1 receptor agonist, in patients with type 2 diabetes: a randomised, placebo-controlled and active comparator-controlled phase 2 trial. *Lancet* **392**, 2180-2193 (2018).
14. A. Pocai *et al.*, Glucagon-like peptide 1/glucagon receptor dual agonism reverses obesity in mice. *Diabetes* **58**, 2258-2266 (2009).
15. A. Pocai, Unraveling oxyntomodulin, GLP1's enigmatic brother. *J Endocrinol* **215**, 335-346 (2012).
16. B. D. Kerr, P. R. Flatt, V. A. Gault, Effects of gamma-glutamyl linker on DPP-IV resistance, duration of action and biological efficacy of acylated glucagon-like peptide-1. *Biochem Pharmacol* **80**, 396-401 (2010).
17. A. Muppidi *et al.*, Design of Potent and Proteolytically Stable Oxyntomodulin Analogs. *ACS Chem Biol* **11**, 324-328 (2016).
18. V. K. Bhat, B. D. Kerr, P. R. Flatt, V. A. Gault, A novel GIP-oxyntomodulin hybrid peptide acting through GIP, glucagon and GLP-1 receptors exhibits weight reducing and anti-diabetic properties. *Biochem Pharmacol* **85**, 1655-1662 (2013).
19. C. Parthier *et al.*, Crystal structure of the incretin-bound extracellular domain of a G protein-coupled receptor. *Proc Natl Acad Sci U S A* **104**, 13942-13947 (2007).
20. C. R. Underwood *et al.*, Crystal structure of glucagon-like peptide-1 in complex with the extracellular domain of the glucagon-like peptide-1 receptor. *J Biol Chem* **285**, 723-730 (2010).

21. S. Runge, H. Thogersen, K. Madsen, J. Lau, R. Rudolph, Crystal structure of the ligand-bound glucagon-like peptide-1 receptor extracellular domain. *J Biol Chem* **283**, 11340-11347 (2008).
22. R. S. Kuna *et al.*, Glucagon-like peptide-1 receptor-mediated endosomal cAMP generation promotes glucose-stimulated insulin secretion in pancreatic beta-cells. *Am J Physiol Endocrinol Metab* **305**, E161-170 (2013).
23. S. B. Girada *et al.*, Galphas regulates Glucagon-Like Peptide 1 Receptor-mediated cyclic AMP generation at Rab5 endosomal compartment. *Mol Metab* **6**, 1173-1185 (2017).
24. J. T. Patterson, P. Li, J. W. Day, V. M. Gelfanov, R. D. Dimarchi, A hydrophobic site on the GLP-1 receptor extracellular domain orients the peptide ligand for signal transduction. *Mol Metab* **2**, 86-91 (2013).
25. P. Y. Yang *et al.*, New Generation Oxyntomodulin Peptides with Improved Pharmacokinetic Profiles Exhibit Weight Reducing and Anti-Steatotic Properties in Mice. *Bioconjug Chem* **31**, 1167-1176 (2020).
26. M. M. Fletcher *et al.*, Glucagon-like peptide-1 receptor internalisation controls spatiotemporal signalling mediated by biased agonists. *Biochem Pharmacol* **156**, 406-419 (2018).
27. T. Shibasaki *et al.*, Essential role of Epac2/Rap1 signaling in regulation of insulin granule dynamics by cAMP. *Proc Natl Acad Sci U S A* **104**, 19333-19338 (2007).
28. S. Seino, Cell signalling in insulin secretion: the molecular targets of ATP, cAMP and sulfonylurea. *Diabetologia* **55**, 2096-2108 (2012).
29. A. Gucek *et al.*, Fusion pore regulation by cAMP/Epac2 controls cargo release during insulin exocytosis. *Elife* **8** (2019).
30. J. S. Bogan, Y. Xu, M. Hao, Cholesterol accumulation increases insulin granule size and impairs membrane trafficking. *Traffic* **13**, 1466-1480 (2012).
31. R. E. Gimeno, D. A. Briere, R. J. Seeley, Leveraging the Gut to Treat Metabolic Disease. *Cell Metab* **31**, 679-698 (2020).
32. R. J. Samms *et al.*, GIPR agonism mediates weight-independent insulin sensitization by tirzepatide in obese mice. *J Clin Invest* **131** (2021).
33. T. Min, S. C. Bain, The Role of Tirzepatide, Dual GIP and GLP-1 Receptor Agonist, in the Management of Type 2 Diabetes: The SURPASS Clinical Trials. *Diabetes Ther* **12**, 143-157 (2021).
34. J. Rosenstock *et al.*, Efficacy and safety of a novel dual GIP and GLP-1 receptor agonist tirzepatide in patients with type 2 diabetes (SURPASS-1): a double-blind, randomised, phase 3 trial. *Lancet* **398**, 143-155 (2021).
35. J. P. Frias *et al.*, Tirzepatide versus Semaglutide Once Weekly in Patients with Type 2 Diabetes. *N Engl J Med* **385**, 503-515 (2021).
36. A. Slomski, Tirzepatide Safely Reduces Blood Glucose, Weight in Type 2 Diabetes. *JAMA* **326**, 691 (2021).
37. B. Khoo, T. M. Tan, Surpassing insulin glargine in type 2 diabetes with tirzepatide. *Lancet* 10.1016/S0140-6736(21)02279-0 (2021).
38. L. L. Baggio, D. J. Drucker, Glucagon-like peptide-1 receptor co-agonists for treating metabolic disease. *Mol Metab* **46**, 101090 (2021).
39. C. J. Bailey, Tirzepatide: a new low for bodyweight and blood glucose. *Lancet Diabetes Endocrinol* **9**, 646-648 (2021).
40. L. Zhao *et al.*, Design, screening and biological evaluation of novel fatty acid chain-modified oxyntomodulin-based derivatives with prolonged glucose-lowering ability and potent anti-obesity effects. *Org Biomol Chem* **17**, 7760-7771 (2019).
41. F. S. Willard *et al.*, Tirzepatide is an imbalanced and biased dual GIP and GLP-1 receptor agonist. *JCI Insight* **5** (2020).

42. S. R. Hoare, Mechanisms of peptide and nonpeptide ligand binding to Class B G-protein-coupled receptors. *Drug Discov Today* **10**, 417-427 (2005).
43. J. W. Neidigh, R. M. Fesinmeyer, K. S. Prickett, N. H. Andersen, Exendin-4 and glucagon-like-peptide-1: NMR structural comparisons in the solution and micelle-associated states. *Biochemistry* **40**, 13188-13200 (2001).
44. M. Wolff *et al.*, A Conserved Hydrophobic Moiety and Helix-Helix Interactions Drive the Self-Assembly of the Incretin Analog Exendin-4. *Biomolecules* **11** (2021).
45. J. G. Lee *et al.*, Replacement of the C-terminal Trp-cage of exendin-4 with a fatty acid improves therapeutic utility. *Biochem Pharmacol* **151**, 59-68 (2018).
46. B. Jones *et al.*, Targeting GLP-1 receptor trafficking to improve agonist efficacy. *Nat Commun* **9**, 1602 (2018).
47. A. Marzook *et al.*, Evaluation of efficacy- versus affinity-driven agonism with biased GLP-1R ligands P5 and exendin-F1. *Biochem Pharmacol* **190**, 114656 (2021).
48. Y. Nakatani *et al.*, Effect of GLP-1 receptor agonist on gastrointestinal tract motility and residue rates as evaluated by capsule endoscopy. *Diabetes Metab* **43**, 430-437 (2017).
49. S. Urva *et al.*, The novel dual glucose-dependent insulinotropic polypeptide and glucagon-like peptide-1 (GLP-1) receptor agonist tirzepatide transiently delays gastric emptying similarly to selective long-acting GLP-1 receptor agonists. *Diabetes Obes Metab* **22**, 1886-1891 (2020).
50. Q. Zhang *et al.*, The glucose-dependent insulinotropic polypeptide (GIP) regulates body weight and food intake via CNS-GIPR signaling. *Cell Metab* **33**, 833-844 e835 (2021).
51. S. Gremlich *et al.*, Cloning, functional expression, and chromosomal localization of the human pancreatic islet glucose-dependent insulinotropic polypeptide receptor. *Diabetes* **44**, 1202-1208 (1995).
52. D. V. Waterhous, W. C. Johnson, Jr., Importance of environment in determining secondary structure in proteins. *Biochemistry* **33**, 2121-2128 (1994).
53. S. M. Kelly, T. J. Jess, N. C. Price, How to study proteins by circular dichroism. *Biochim Biophys Acta* **1751**, 119-139 (2005).
54. S. Asalla *et al.*, Restoring Mitochondrial Function: A Small Molecule-mediated Approach to Enhance Glucose Stimulated Insulin Secretion in Cholesterol Accumulated Pancreatic beta cells. *Sci Rep* **6**, 27513 (2016).
55. K. J. Livak, T. D. Schmittgen, Analysis of relative gene expression data using real-time quantitative PCR and the 2(-Delta Delta C(T)) Method. *Methods* **25**, 402-408 (2001).
56. U. S. Pettersson, T. B. Walden, P. O. Carlsson, L. Jansson, M. Phillipson, Female mice are protected against high-fat diet induced metabolic syndrome and increase the regulatory T cell population in adipose tissue. *PLoS One* **7**, e46057 (2012).

Table 1: In vitro GLP-1R, GIPR, GCGR activity of peptide analogs

No	Peptide	Constituent amino acids	GLP-1R		GIPR		GCGR	
			% liraglutide activity	SD	% GIP activity	SD	% Oxm activity	SD
1	**Liraglutide**	**HAEGTFTSDVSSYLEGQAAKcEFIAWLVKGRG**	**100**	**6.7**	24.08	2.13	10.90	0.13
2	**GIP**	**YAESTFISDYSIAMDKIHQQDFVNWLLAQKGKK NDWKHNITQ**	31.86	3.8	**100**	**6.6**	23.39	1.74
3.	**Exendin 4**	**HGEGTFTSDLSKQMEEEAVRLFIEWLKNGGPSS GAPPPS-NH2**	**140.24**	**3.15**	**28.20**	**1.17**	21.45	1.49
4	**Oxyntomodulin**	**HSQGTFTSDYSKYLDSRRAQDFVQWLMNTKRN RNNIA**	**96.26**	**0.96**	30.76	1.68	100	1.4
5	**I-M-150844**	**HGEGTFTSDVF**	21.66	2.69	15.55	2.37	6.49	0.45
6.	**I-M-150845**	**YGEGTFTSDYSIAMDKIHQQDFVNWLVKGRG (3563.9)**	**76.78**	**6.32**	**86.9**	**13.4**	11.5	0.9
7	**I-M-150846**	**YGEGTFTSDYSIAMDKIHQQDFVNWLMNTKRNR NNIA (4379.8)**	38.21	0.6	**65.65**	**6.7**	7.14	0.4
8	**I-M-150847**	**YGEGTFTSDLSKQMEEEAVRLFIEWLMNTKRNR NNIA (4392.88)**	**122.95**	**2.0**	**108.0**	**5.1**	14.93	1.68
9	**Basal**	**Phosphate Basal Saline**	29.96	1.5	16.43	**5.0**	8.12	0.2

Table legend: The activity of the peptide analogs in vitro in GLP-1R, GIPR, and GCGR assay system as measured by cyclic AMP responsive element luciferase reporter assay. % Liraglutide activity is defined as the normalized relative luciferase units generated upon treatment of HEK –GLP-1R expressing cells with 1µM liraglutide. % GIP activity is defined as the normalized relative luciferase units generated upon treatment of HEK –GIPR expressing cells with 10µM IUB 68. % GCGR activity is

defined as the normalized relative luciferase units generated upon treatment of HEK – GCGR expressing cells with 10μM Oxyntomodulin. Oxm =Oxyntomodulin. The numbers in brackets represent the molecular mass of the peptide. The data represent the means ± SD of the experiment carried out in duplicate in each heterologous assay system. The amino acids that correspond to liraglutide exendin-4, oxyntomodulin, and GIP are colored green, black, blue, and red respectively

1

Figure 1

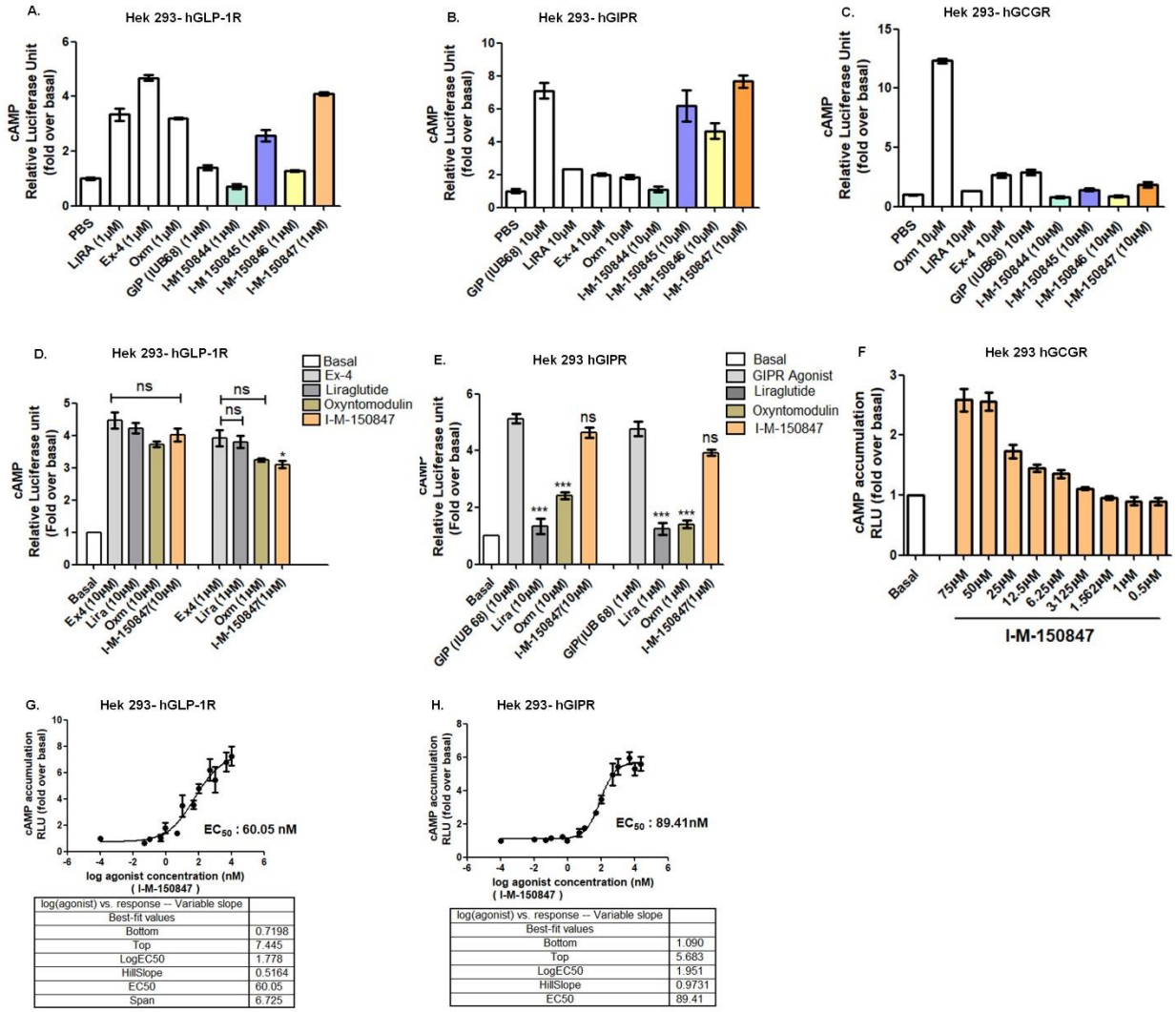

log(agonist) vs. response -- Variable slope	
Best-fit values	
Bottom	0.7198
Top	7.445
LogEC50	1.778
HillSlope	0.5164
EC50	60.05
Span	6.725

log(agonist) vs. response -- Variable slope	
Best-fit values	
Bottom	1.090
Top	5.683
LogEC50	1.951
HillSlope	0.9731
EC50	89.41

2

3

4

5

1

Figure 2.

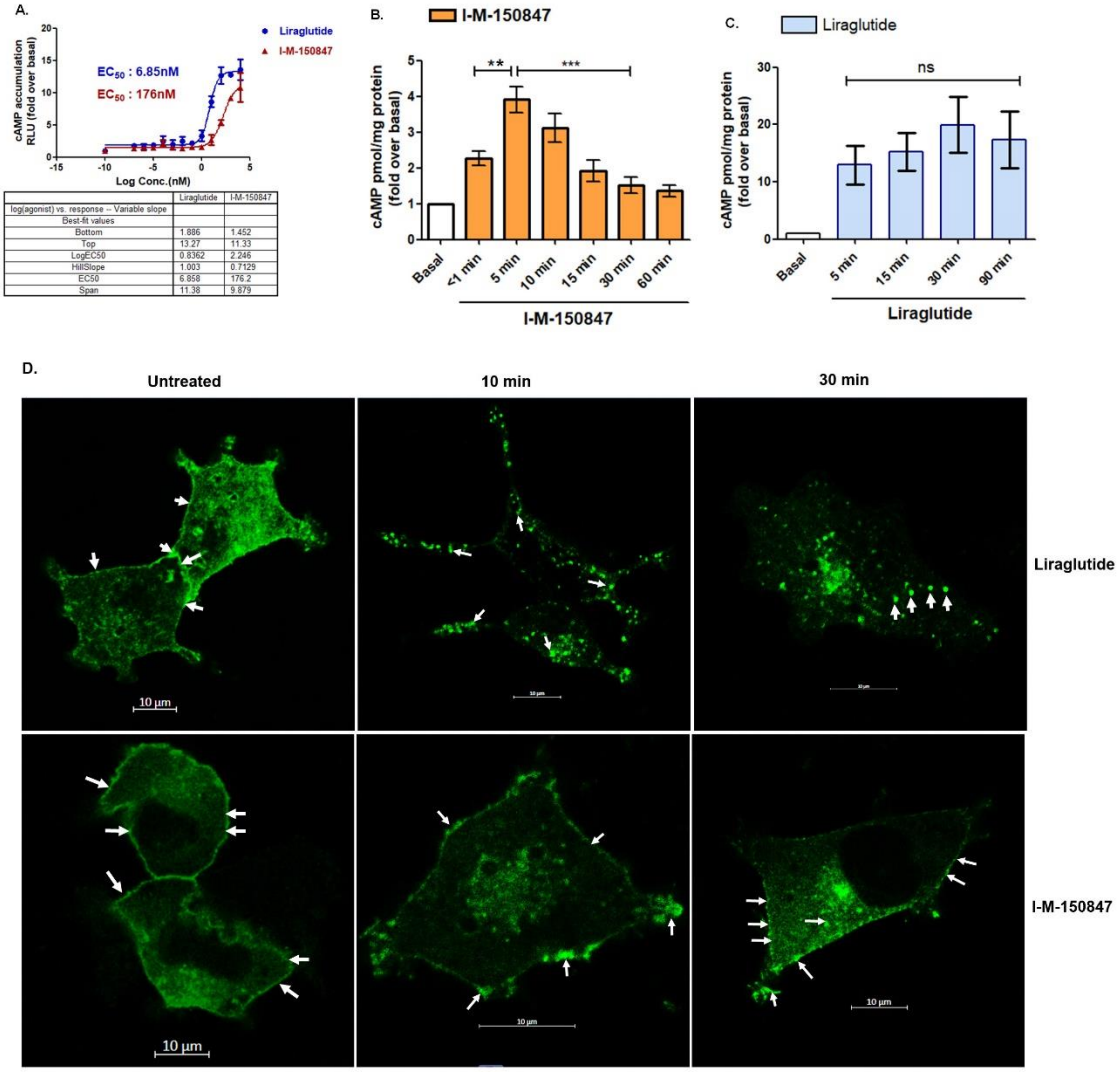

	Liraglutide	I-M-150847
log(agonist) vs. response -- Variable slope		
Best-fit values		
Bottom	1.886	1.452
Top	13.27	11.33
LogEC50	0.8362	2.246
HillSlope	1.003	0.7129
EC50	6.858	176.2
Span	11.38	9.879

2

3

4

5

6

1

Figure 3.

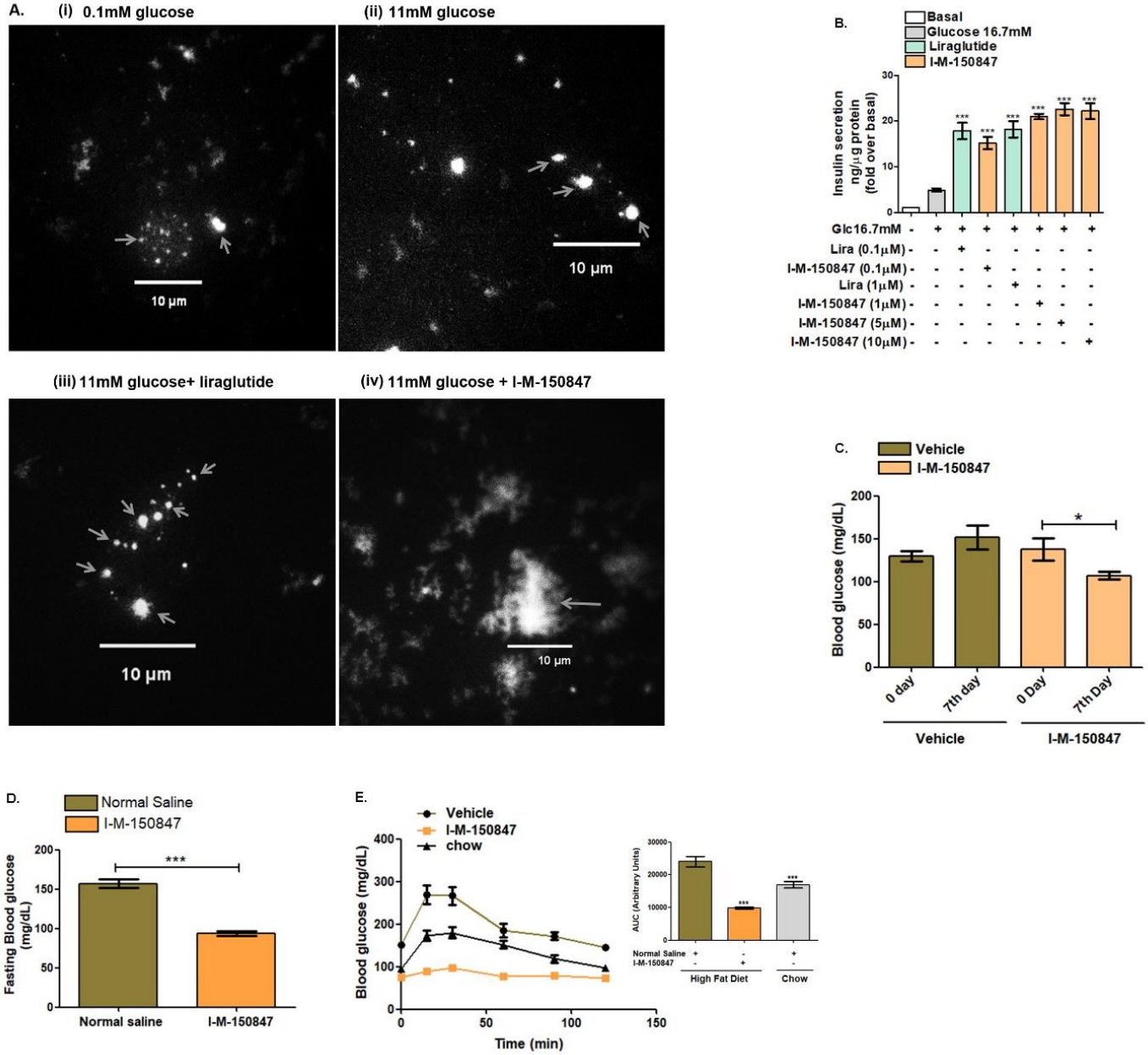

2

3

4

5

Figure 4.

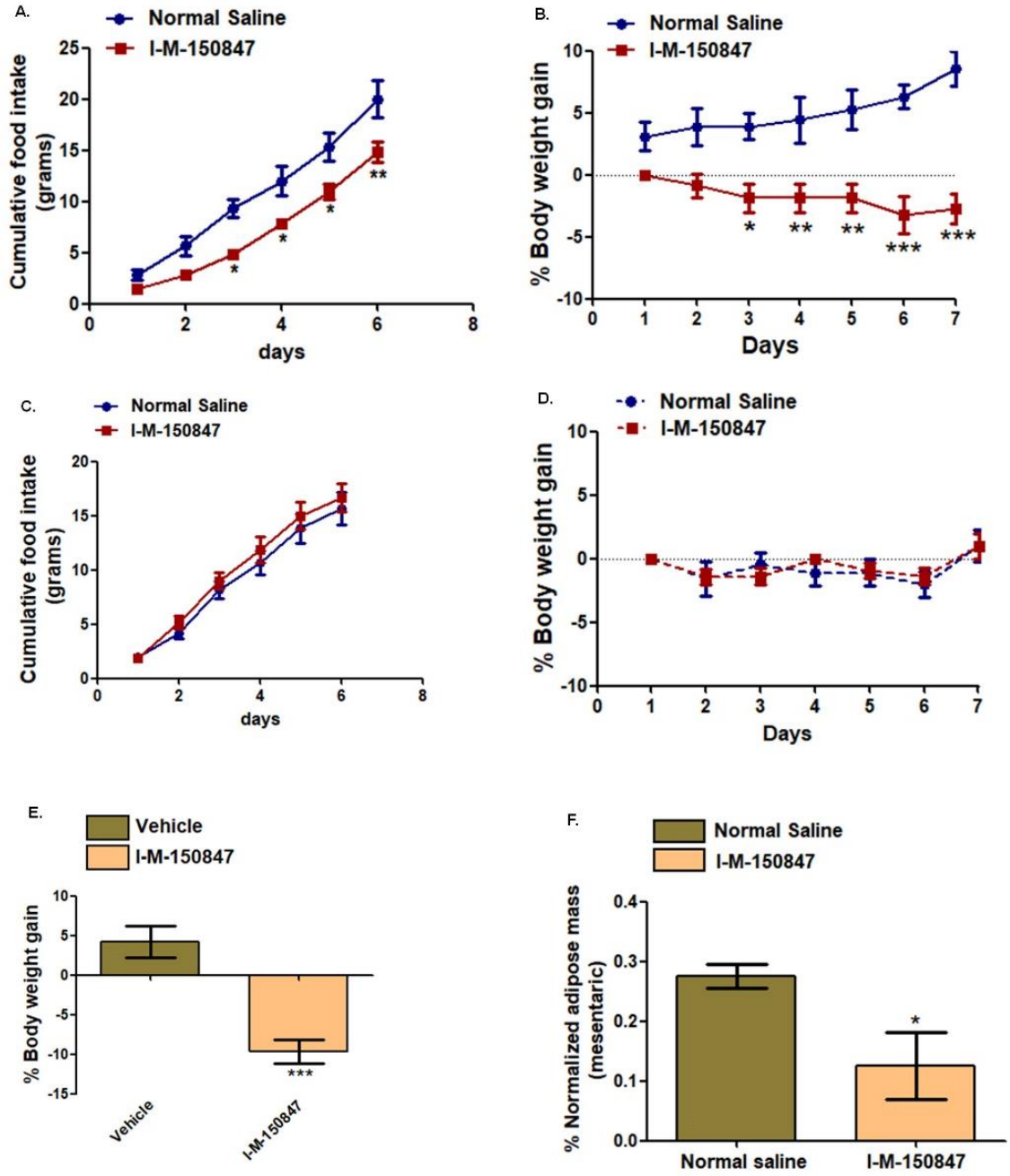

1

2

3

4